# EPR of tungsten impurities in $KTiOPO_4$ single crystals grown from molten tungstate solutions

D. Bravo
*Departamento de Física de Materiales, Facultad de Ciencias, C-IV, Universidad Autónoma de Madrid, Cantoblanco, E-28049 Madrid, Spain*

X. Ruiz and F. Díaz
*Laboratorio de Física Aplicada y Cristalografía, Universidad Rovira y Virgili, Tarragona, Spain*

F. J. López
*Departamento de Física de Materiales, Facultad de Ciencias, C-IV, Universidad Autónoma de Madrid, Cantoblanco, E-28049 Madrid, Spain*

(Received 17 February 1995)

The presence of tungsten impurities in $KTiOPO_4$ (KTP) crystals grown from molten tungstate solutions has been observed by means of electron paramagnetic resonance (EPR) at 90 K. The angular dependence of the EPR signals and their behavior under thermal treatments allow us to distinguish two tungsten centers. The analysis of the measured **g** and hyperfine matrices for both centers indicates that the signals are due to $W^{5+}$ located at the two titanium sites of the KTP structure. Moreover, it is shown that pentavalent tungsten is incorporated as the tungstenyl $WO^{3+}$ ion, whose formation is favored by the existence of one short "titanyl" Ti-O bond for each site. The results for the tungstenyl ion are compared to those for other oxycations previously studied in KTP. On the other hand, the intensity changes induced on the EPR signals by the thermal treatments indicate that most tungsten impurities enter the Ti1 site in the hexavalent state for the as-grown crystals. Besides, the presence of some tetravalent tungsten at the Ti2 site created by the reducing treatment is inferred.

## I. INTRODUCTION

Potassium titanyl phosphate ($KTiOPO_4$ or KTP) is a remarkable nonlinear optic and electro-optic material.[1] It is often used for frequency doubling of laser radiation.[1,2] Recently, KTP has attracted attention as substrate in producing optical waveguides by ion exchange[1,3] and ion implantation.[4] The degree of difficulty involved in obtaining large single crystals of high optical quality for these applications, led Ballman *et al.*[5] to propose a flux or molten solution growth process utilizing tungstate melts as the solvent. This method reduces the melt viscosity and volatility,[5–7] making the crystal growth process easier and supplying large crystals free of inclusions. However, tungsten is incorporated into the crystal, giving rise to visible striations and sectors caused by temperature fluctuations in the growth process.[8]

The presence of intrinsic defects and impurities in KTP crystals has a critical influence on the above-mentioned applications. For waveguide applications, the ionic conductivity (associated to potassium vacancies) can be conveniently reduced utilizing the doping of trivalent ions (Ga and Al) on the Ti sites[9,10] and tetravalent ions (Si) on the P sites.[10] On the other hand, the susceptibility of KTP crystals to optical[11,12] and electric-field damage[13] has been related to the presence of $Ti^{3+}$ defects.[12,13] Besides, the susceptibility to "grey track" formation,[11,12] involved in laser damage, has been found to be maximum in crystals grown from tungsten-based solvents.[12]

Despite the important role that tungsten can play on the physical properties of KTP and its isomorphs,[14] no definite research on the possible oxidation states and structural position of this metal in KTP crystals has been carried out. It has, however, been assumed[8] that tungsten occupies the titanium positions, which is based on the similar structures of $NaWO_2PO_4$ and $KTiOPO_4$.[8,15]

The electron-paramagnetic-resonance (EPR) technique is able to provide rather detailed information on the chemical and electronic structure of paramagnetic defects. This technique has been used in KTP to study a radiation-induced hole center,[16] various $Ti^{3+}$ defect centers,[13,17–19] as well as several centers due to transition-metal-ion impurities, namely $Fe^{3+}$, $Cr^{3+}$ (Ref. 20), $VO^{2+}$ (Ref. 21), $V^{4+}$ (Refs. 22,23), $Mo^{5+}$ (Ref. 24), and $Rh^{2+}$ (Ref. 19). All these impurities have been found by EPR to be located at the Ti position.

Recently, the effect of the thermal treatments on KTP crystals grown from molten tungstate solutions has been disclosed by means of optical and EPR investigations.[18] Along that research, changes in the valence state of several impurities (Fe, Rh, and W) were observed. This work presents the EPR results obtained at 90 K for two paramagnetic centers associated to tungsten impurities in KTP single crystals. Each center corresponds to one of the two available Ti sites in the KTP structure (see the next section), although most tungsten enters one of them. Moreover, the observed EPR signals are ascribed to pentavalent tungsten, which is forming the tungstenyl $WO^{3+}$

 

ion. The results are discussed and compared to those for other $nd^1$ ions studied in KTP.

## II. CRYSTAL STRUCTURE

The crystal structure of KTP was solved by Tordjman, Masse, and Guitel.[15] Recently, slightly different structural parameters have been reported.[25] The structure is orthorhombic, with space group $Pna2_1$ (Refs. 15,25) and lattice constants $a=12.819$ Å, $b=6.399$ Å, and $c=10.584$ Å.[25] There are two crystallographically distinct sites for each of the cations in the unit cell (labeled as Ti1, Ti2, K1, K2, P1, and P2) and ten independent oxygen positions (labeled as O1–O8, OT1, and OT2). All sites have point symmetry $C_1$. Figure 1 shows the two sites for titanium, Ti1 and Ti2. In addition, each ion is replicated in four positions within the unit cell by the symmetry operations of the space group (identity, two glide planes perpendicular to the $a$ and $b$ axes, respectively, and one screw axis coincident with the $c$ axis). Accordingly, the unit cell consists of eight formula $KTiOPO_4$.

The structure is characterized by corner-linked $TiO_6$ octahedra. Oxygens OT1 and OT2 form the links, while the four others belong to phosphate groups (see Fig. 1). Titanium ions Ti1 and Ti2 are involved together with the linking oxygens in a chain (—OT2–Ti1—OT1–Ti2—OT2–), with alternating short (–, ≈1.72 Å) "titanyl" bonds and long (—, ≈2 Å) bonds. The large optical nonlinearity in KTP has been attributed mainly to the presence of these two short Ti-O bonds in the chain.[1] The triclinic symmetry of the oxygen arrangement around Ti1 and Ti2 sites can be approximated to tetragonal $C_{4v}$ symmetry, as the four remaining equatorial Ti-O bonds, almost perpendicular to the short bond, have more similar lengths.[15,19,25] The $PO_4$ tetrahedra are distorted to some extent, but are more regular than the $TiO_6$ octahedra. Potassium K1 is eightfold coordinated by oxygen and K2 is ninefold coordinated. They occupy one-dimensional channels along the $c$ axis, which facilitates the ionic conduction of the K ions along this direction.[1]

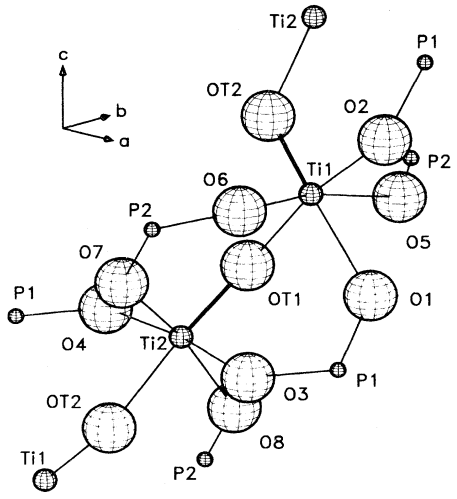


FIG. 1. Partial scheme of the KTP structure showing the crystal axes $a$, $b$, and $c$. The two titanium sites, together with their first and second coordination spheres are shown. Potassium ions are not included for the sake of clarity. The short "titanyl" bonds are depicted with thick lines.

## III. EXPERIMENTAL DETAILS

The KTP crystals used in the present work have been grown by a top seeded solution growth from W-rich melts in the Crystal Growth Laboratory of Universidad Rovira y Virgili, Tarragona. KTP single crystals were obtained from mixtures of $42K_2O$:/$14P_2O_5$:$14TiO_2$:$30WO_3$, melted in a Pt-10% Rh crucible and cooled from 914 °C to 872 °C at a rate of 0.2 °C/h. The crystal composition has been determined by electron microprobe analysis in a previous work.[18] The most remarkable outcome for our as-grown crystals is a 10% K deficiency[18] with respect to stoichiometric KTP. The main impurity content in these crystals has been obtained by means of electron microprobe and atomic absorption spectroscopy analysis.[18] The average results are Fe≈300 ppm; Co≈200 ppm; Si ≈3000 ppm; Rh≈2000 ppm; W≈3000 ppm. (Note the misprint in Table I of Ref. 18: $\times 10^{16}$ should read $\times 10^{6}$.)

Crystal orientation was achieved by taking a number of Laue x-ray-diffraction patterns. KTP samples were subsequently sawn with their faces perpendicular to the crystal axes $a$, $b$, and $c$ of KTP, so that the angular dependence of the EPR spectra can be studied conveniently.

Thermal treatments were performed by heating the samples in vacuum or air using conventional furnaces and ceramic tubes. In Ref. 18 the treatments in vacuum and air have been associated to reduction and oxidation treatments, respectively. The treatments consist of the following steps.

(i) First, the KTP samples were reduced by means of vacuum annealing at 650 °C for half an hour.

(ii) Subsequent oxidation has been carried out by heating the samples in air at 600 °C by increasing periods of time.

EPR spectra were recorded at 90 K with a Bruker ESP 300E X-band spectrometer using field modulation of 100 kHz. A microwave-frequency counter (Hewlett-Packard 5342A) and a NMR gaussmeter (Bruker ER 035M) were used for accurate determination of the spectrometer frequency and magnetic field, respectively. The crystals were mounted on a goniometer for measurements of the angular dependence of the EPR spectra.

## IV. RESULTS

### A. Features of the EPR spectra

The signals are undetectable at room temperature, but easily observed at 90 K, having a peak-to-peak derivative linewidth of 25–35 G at this temperature. Figure 2 shows the EPR spectra of tungsten impurities taken with the magnetic field **H** parallel to the $b$ axis of the crystal for different states of the KTP samples. The spectrum consists of two groups of lines, hereafter denoted W1 and

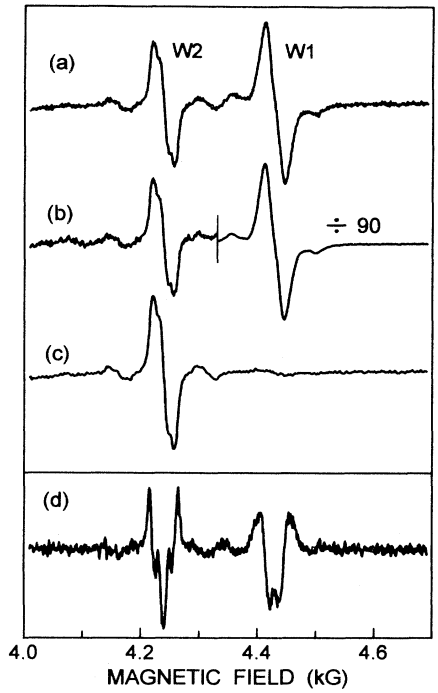


FIG. 2. EPR first derivative spectra of tungsten impurities in KTP, recorded at 90 K with the magnetic field oriented along the crystal *b* axis. All the lines are fourfold degenerate for this orientation. The two groups of lines are denoted W1 and W2. (a) as-grown samples; (b) reduced samples for half an hour at 650 °C; (c) oxidized samples at 600 °C during three hours or longer periods; (d) second derivative spectrum for as-grown samples, obtained from spectrum (a).

W2, with similar structure. Each group is composed of a central main line flanked by weaker lines which are spaced symmetrically to each side of the main line. The groups show similar features when **H** is parallel to the *a* and *c* axes of the crystal, but they appear at different resonance fields. Moreover, Figs. 2(a)–2(c) show that the intensity changes induced by the thermal treatments on the main line and on the weaker accompanying doublets are proportional. Therefore, the central main line should arise from the even isotopes of tungsten, while the weaker lines would result from hyperfine (HF) interaction with the nuclear spin $I=\frac{1}{2}$ of the 14.3% abundant $^{183}W$ isotope. From the isotopic abundance, the intensity of the main line relative to one HF component would be 12.0. The results of a number of intensity measurements for both groups taken at different magnetic field orientations give a relative strength of 13±2. This is regarded as satisfactory evidence that groups W1 and W2 are due to tungsten impurities in KTP.

On the other hand, further structure of the signals can be appreciated on the even isotope lines as well as on the accompanying HF doublets (see Fig. 2). To better observe such structure the second derivative of the spectra has been obtained. As an example, Fig. 2(d) shows the results for **H** oriented along the crystal *b* axis. Group W1 shows a doublet structure which is well observed for **H** lying in the crystal plane *ab*, but is lost for **H** more than ≈20° outside this plane. The doublet has a separation of 12±1 G and 16±2 G for **H** parallel to the crystal axes *a* and *b*, respectively. Group W2 shows a triplet structure well observed for **H** along the crystal axes *b* and *c*, with separations of 14±2 G and 19±2 G, respectively, while more complicated splittings appear for other orientations. Even though it was not possible to perform a complete analysis of the splittings, the structure is very likely superhyperfine (SHF) structure caused by $^{31}P$ nuclei ($I=\frac{1}{2}$) as close neighbors of tungsten impurities. Taking into account this structure the individual peak-to-peak derivative linewidth of the tungsten signals would be 15–20 G at 90 K. Moreover, it is probable that observation of the signals at lower temperatures would show up further SHF splitting, as it occurs on the molybdenum EPR spectra measured in KTP.[24]

### B. Thermal treatment effects

The evolution of the EPR spectrum of our KTP samples induced by thermal treatments has already been reported.[18,19] We will focus our attention on the effects that such treatments produce on the EPR signals ascribed to tungsten impurities. These can be summarized as follows.

(i) Reducing the KTP samples gives rise to a strong increase (≈90 times) of group W1 [see Fig. 2(b)] with respect to that exhibited by the as-grown samples [Fig. 2(a)], while group W2 shows no appreciable changes.

(ii) Starting with the reduced samples, we have measured the changes in the spectrum intensity of groups W1 and W2 upon oxidation. Figure 2(c) shows the spectrum for the strongly oxidized state, which is essentially reached after 180 min of heating the samples in air. It is observed that group W1 almost disappears for this state. The detailed evolution of the intensity of both groups is shown in Fig. 3 as a function of oxidation time. The maximum intensity reached by each group is about 65 times larger for W1 than for W2.

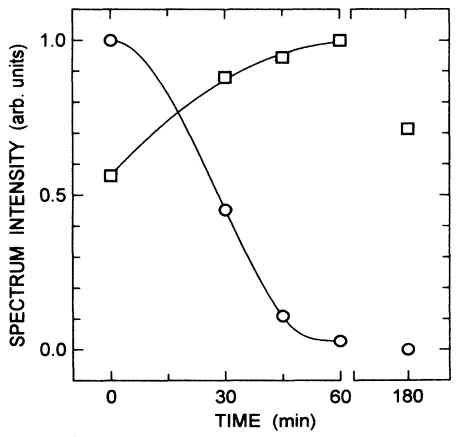


FIG. 3. Normalized evolution of the spectrum intensity of groups W1 (○) and W2 (□) as a function of time of oxidation treatment. The curves have been drawn to guide the eye. The maximum intensity before normalization was 65 times larger for W1 than for W2.

It should be mentioned that the intensity changes induced by the thermal treatments do not involve variations in EPR line positions or line shape. Besides, no new spectral features appear which could be ascribed to other tungsten centers. On the other hand, the as-grown state roughly corresponds to that of strong oxidation, as would be expected from the oxidizing conditions at which the growth process takes place. This was also observed for the other impurities (Fe and Rh) detected in our crystals.[18]

### C. Analysis of the EPR spectra

The remarkable intensity changes undergone by group W1 as compared to W2 under thermal treatments indicate that each group is due to a different center. In order to analyze the centers we have obtained the angular dependence of the EPR spectra in the three crystal planes *ab*, *ac*, and *bc*. Owing to overlapping of the signals of both centers for many orientations of **H**, we have performed measurements for two different states of the samples. Reduced samples have been employed to measure the W1 signals, as they are much more intense than W2 [Fig. 2(b)]. The measurements for W2 have been carried out using the strongly oxidized samples, as the W1 signals disappear for this state [Fig. 2(c)]. The experimental resonance fields of well-defined lines have been plotted for each center in Fig. 4.

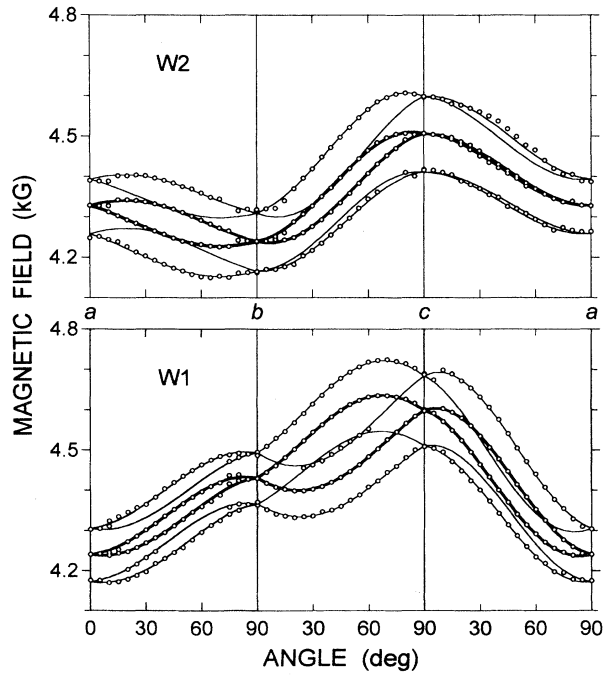


FIG. 4. Angular dependence of the EPR spectrum of tungsten centers W1 and W2 measured at 90 K in the three crystal planes *ab*, *bc*, and *ca* of KTP. Circles represent the experimental resonance fields. Solid lines depict the resonance fields calculated with the fitted parameters given in Table I. Thick lines are used for the even isotopes, and thin lines for the $^{183}$W isotope.

The angular dependences clearly show two different centers, each behaving as a system with effective spin $S'=\frac{1}{2}$ and effective $g$ values lower than 2. For arbitrary directions of **H** with respect to the crystal axes, four groups per each W center can be separately observed, which correspond to four different orientations of each center. The four groups collapse in two doubly degenerate ones for **H** lying in the *ab*, *ac*, or *bc* planes, while they collapse into a fourfold degenerate group for **H** along one of the three crystal axes. This behavior is consistent with the symmetry operations of the KTP structure given in Sec. II.

The EPR spectra of each center and their angular dependence are analyzed using the following spin Hamiltonian appropriate for a center having $S'=\frac{1}{2}$ and $I=\frac{1}{2}$:

$$\hat{\mathcal{H}}=\beta\mathbf{H}\cdot\mathbf{g}\cdot\hat{S}'+\hat{S}'\cdot\mathbf{A}\cdot\hat{I}\ , \tag{1}$$

where the terms represent the electronic Zeeman interaction and the HF interaction, respectively, the parameters having the usual meaning. The nuclear Zeeman interaction has been neglected as it is very small and gives corrections to the EPR line positions lower than the experimental error. The full spin Hamiltonian is used to study the HF components, while only the Zeeman part is necessary for the analysis of the even isotope lines. To analyze the angular dependences in a suitable way, the **g** and **A** matrices in Eq. (1) are expressed in the crystal axes system $(a,b,c)$. In general, the matrices will be nondiagonal in such system. Besides, owing to the low symmetry of the cation sites in KTP, no constraint should be imposed on the matrices. However, they will be considered symmetric, since the standard EPR experiments in low-symmetry complexes are not able to detect asymmetries in the **g** and **A** matrices.[26]

To obtain the **g** matrices for centers W1 and W2 we have employed a program which diagonalizes the $2\times2$ energy matrix for the Zeeman term in Eq. (1) and performs a least-squares procedure. To this aim, for each center we have used 108 independent measurements of even isotope line positions as input data, as well as their corresponding microwave frequencies. The resulting best-fit **g** matrix is subsequently employed to obtain the **A** matrix using a similar procedure, but now the full $4\times4$ energy matrix represented in Eq. (1) is diagonalized. In this case, the input data are 110 measurements of HF line positions, which correspond to the well-defined lines at the outer sides of the angular dependences (see Fig. 4). The best-fit **g** and **A** matrices obtained for each center are now diagonalized, providing the principal values and principal axes $(x,y,z)$ referred to the crystal axes system $(a,b,c)$. The results are given in Table I for one orientation of the principal axes described by direction cosines $[l,m,n]$. The three other orientations correspond to $[\bar{l},m,n]$, $[l,\bar{m},n]$, and $[l,m,\bar{n}]$, according to the symmetry operations of the KTP structure. The errors in the resulting data are obtained from the used least-squares procedure by considering a line position uncertainty of 3–4 G for center W1 and 4–6 G for W2. On the other hand, the matrices in the $(a,b,c)$ system have been used to calculate the solid lines in Fig. 4. For center W1 the average

TABLE I. Spin-Hamiltonian parameters for the two tungsten centers W1 and W2 observed in KTP at 90 K. The HF constants are given in units of $10^{-4}$ $cm^{-1}$. The **g** and **A** matrices are expressed in diagonal form. Labeling of the principal $g$ values has been made by decreasing magnitude. Principal axes of the **A** matrix are labeled according to the closest principal axis of the **g** matrix. Principal axes orientation is given both by direction cosines, $[l,m,n]$, and polar coordinates, $(\theta,\phi)$, referred to the crystal $(a,b,c)$ system (see text).

| | Principal values | | Principal axes | | | | |
|---|---|---|---|---|---|---|---|
| | | | $l$ | $m$ | $n$ | $\theta$ (deg) | $\phi$ (deg) |
| | $g_x$ | 1.6037±0.0006 | 0.980 | −0.147 | 0.133 | 82.4±0.2 | 351.5±0.4 |
| | $g_y$ | 1.5406±0.0008 | 0.185 | 0.917 | −0.352 | 110.6±0.4 | 78.6±0.4 |
| | $g_z$ | 1.4634±0.0008 | −0.071 | 0.370 | 0.926 | 22.1±0.4 | 100.8±0.6 |
| W1 | | | | | | | |
| | $\lvert A_x\rvert$ | 77±3 | 0.781 | −0.282 | 0.558 | 56±2 | 340±10 |
| | $\lvert A_y\rvert$ | 92±2 | 0.285 | 0.955 | 0.083 | 85±4 | 73±6 |
| | $\lvert A_z\rvert$ | 136±3 | −0.556 | 0.094 | 0.826 | 34±2 | 170±5 |
| | | | $l$ | $m$ | $n$ | $\theta$ (deg) | $\phi$ (deg) |
| | $g_x$ | 1.6064±0.0008 | −0.323 | −0.941 | 0.106 | 83.9±0.4 | 251.1±0.8 |
| | $g_y$ | 1.5636±0.0008 | 0.947 | −0.320 | 0.041 | 87.7±0.8 | 341.3±0.8 |
| | $g_z$ | 1.5046±0.0006 | −0.005 | 0.113 | 0.994 | 6.5±0.4 | 92±6 |
| W2 | | | | | | | |
| | $\lvert A_x\rvert$ | 82±4 | −0.257 | −0.776 | 0.576 | 55±2 | 252±15 |
| | $\lvert A_y\rvert$ | 97±3 | 0.943 | −0.332 | −0.027 | 92±7 | 341±7 |
| | $\lvert A_z\rvert$ | 151±3 | 0.212 | 0.536 | 0.817 | 35±2 | 68±6 |

deviations between the experimental and calculated positions are 2.7 G for the even isotope lines and 3.6 G for the HF lines, while for center W2 these are 3.5 and 5.6 G, respectively. The deviations mainly arise from some degree of inaccuracy in determining EPR line positions because of the additional $^{31}P$ SHF structure on the signals. Nevertheless, Fig. 4 shows good agreement between experiment and theory.

It should be noted that there is an ambiguity involved in the method employed to determine the **g** matrix by means of the three angular dependences given. It arises because there are eight sign combinations for the three off-diagonal elements of the **g** matrix. The eight combinations fall into two sets of four, based on whether the sign of the product of the three off-diagonal elements is positive or negative. No ambiguity exists within a set, as the principal $g$ values are the same and each of the four combinations corresponds to one of the four symmetry-related orientations of the center in the KTP structure. However, one has to decide which is the correct set, either with positive or negative product. The sign choice is based on examination of the EPR spectra recorded with the magnetic field lying in a skew plane. In our case, the plane chosen contains the $b$ axis and crosses the $ac$ plane at $\approx 39°$ with the $c$ axis. The agreement of the calculated line positions with the experimental ones is excellent using the fitted **g** matrix for the set with positive product for both W1 and W2 centers (given in Table I), while it fails for the set with negative product.

On the other hand, the relative sign of the **A**-matrix elements is obtained in the fitting procedure. The best fit is achieved for the sign combinations given in Table I, i.e., the same relative sign for all three principal values, while trying other sign combinations always gives worse fits. However, their absolute sign cannot be determined from the spectrum of a system having $S=\frac{1}{2}$ and $I=\frac{1}{2}$ because of the absence of fine structure.[27]

## V. DISCUSSION AND CONCLUSIONS

### A. Impurity location

The results in the preceding section show that the EPR signals arise undoubtedly from tungsten impurities in KTP, which are present in two crystallographically nonequivalent sites. To locate the tungsten ions in the KTP lattice we first note the similar orientations of the **g** matrices for the tungsten centers (Table I) and those measured for the various $Ti^{3+}$ centers observed in KTP.[13,18] For all centers of both ions the principal $z$ axis (that corresponding to the lowest $g$ value, as defined here) has a large component along the crystal $c$ axis. This suggests that tungsten ions would occupy the Ti sites. However, the **g** matrices alone do not allow us to propose it definitely because of two reasons. First, one would expect to observe nearly axial **g** matrices owing to the approximate $C_{4v}$ symmetry of the Ti sites (see Sec. II), but this is not the case (Table I). Second, comparison of the principal axes of the **g** matrix with all Ti-O bond directions in the unit cell always fails. Such disappointing results are likely due to the low triclinic symmetry of the sites in KTP, which can play an important role on the **g** matrices. In fact, the principal axes for the **g** and **A** matrices are noncoincident (see Table I), which is a typical low-symmetry effect.[26] Moreover, it has been shown[28] that the orientation of the principal axes of the **g** matrix

in low-symmetry complexes may be quite different from the metal-ligand directions.

The location of tungsten impurities can be better inferred from the principal axes of the **A** matrix. This is because the HF interaction depends largely upon the basic nature of the ground state, and it is thought[29] that these axes will lie close to the metal-ligand directions. According to this, we have compared the principal axes of the **A** matrix for both tungsten centers to all cation-oxygen directions in the unit cell of KTP. No positive result is found for the cases of potassium or phosphorus. However, the principal $z$ axis of the **A** matrix for centers W1 and W2 is close to the direction of the shortest Ti1-OT2 and Ti2-OT1 bonds, respectively. This can be observed in Fig. 5, where the orientation of the principal axes of the **A** matrices given in Table I are drawn in stereographic projection together with the orientations of the Ti-O bonds for the Ti1 and Ti2 sites. Also, the **A** matrices show a remarkable axiallity along their corresponding $z$ axes (Table I), as expected from the approximate $C_{4v}$ symmetry of the Ti sites. Furthermore, since both Ti sites exhibit nearly the same Ti-O bond distances and angles within the respective $TiO_6$ octahedron,[15,25] this should be reflected on similar principal values for both centers, as observed. Finally, we note that the $(Ti1)O_6$ and the $(Ti2)O_6$ octahedra are approximately related in the unit cell by an average rotation of $99\pm4°$ (or $81\pm4°$) around the crystal $c$ axis, as can be seen from their orientations in Fig. 5. Such a rotation is indeed observed on the relative orientations of the axes for both **A** matrices. In fact, the principal axes $x$, $y$, and $z$ of center W2 are approximately related to the corresponding axes of center W1 by a positive rotation around the $c$ axis of 88°, 92°, and 102°, respectively (see Table I).

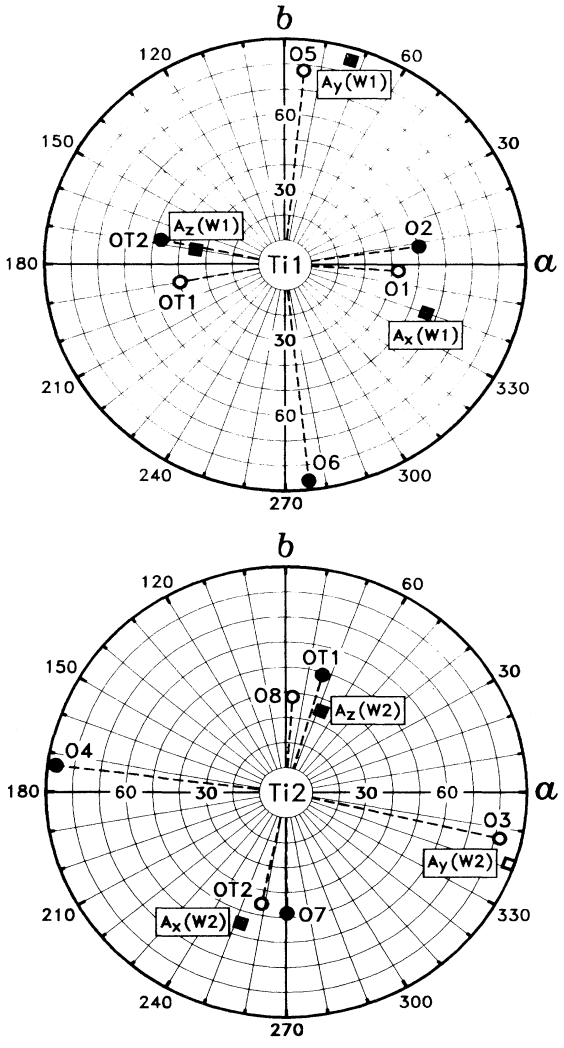


FIG. 5. Stereographic projections in the crystal plane $ab$ of KTP of the principal axes (Table I) of the **A** matrices of tungsten centers (■, □), together with those of the Ti-O bond directions (●, ○). Full (open) symbols are used for directions in the upper (lower) hemisphere.

We therefore conclude that centers W1 and W2 can be unambiguously assigned to tungsten ions located at the Ti1 and Ti2 sites, respectively. This conclusion agrees with the previous assumption of Shumov *et al.*,[8] who proposed that tungsten impurities occupy the Ti sites on the basis of the similar structures of $NaWO_2PO_4$ and $KTiOPO_4$ (Ref. 15).

### B. Valence state of tungsten impurities

The valence state of tungsten must be the same for both paramagnetic centers W1 and W2, as the impurity is located at similar crystallographic sites and the centers show very similar spin-Hamiltonian parameters (Table I). Because of the comparable size and properties of tungsten and molybdenum ions, one would anticipate that $W^{5+}$ gives rise to the observed EPR spectra, as molybdenum has been observed in KTP by means of EPR in the pentavalent state.[24] The $W^{5+}$ ion should be a good fit to the $Ti^{4+}$ site and indeed it is found to substitute for $Ti^{4+}$ in $TiO_2$ (Ref. 30). Moreover, since all $g$ values are smaller than 2,[27,31] and since the spectrum does not show any fine structure, centers W1 and W2 can be temptatively ascribed to $W^{5+}$ ($5d^1$) ions.

At this point, one should consider that $W^{3+}$ ($5d^3$) ions can also give rise to a paramagnetic center with effective spin $S'=\frac{1}{2}$. The fourfold degeneracy of the ground state $^4A_2$ of octahedral $W^{3+}$ ($S=\frac{3}{2}$) can be lifted by a large zero-field splitting to give a low-lying Kramers doublet with $S'=\frac{1}{2}$. For axial symmetries the effective $g$ values of the ground doublet are predicted to be about $g_{\parallel}=2$ or 6 and $g_{\perp}=4$ or 0, respectively, depending on the sign of the zero-field splitting parameter $D$ (Ref. 31). In the orthorhombic cases one $g$ value larger than 4 is always predicted,[31] so that $W^{3+}$ ions should show at least one $g$ value clearly larger than 2, but this is not our case. Furthermore, the considerable anisotropic character of the HF interaction (Table I) does not favor assignment to $W^{3+}$ ions. This is because for $nd^3$ ions the first-order approximation of the electron-nuclear dipolar contribution to the HF interaction vanishes and nearly isotropic HF matrices are usually observed.[32] Hence we discard the possibility of $W^{3+}$ ions as the origin of the observed EPR spectra.

To confirm that centers W1 and W2 are due to $W^{5+}$ ions and to obtain further information on their nature, the $g$ and $A$ values measured here are compared in Table II to EPR data available in the literature for pentavalent tungsten in several hosts. The spin-Hamiltonian parameters for various $nd^1$ ions in KTP are also listed at the end of Table II. Inspection of the data shows that the $W^{5+}$ ion usually has $g$ values lower than 2, as obtained here for KTP. Also, the mean $g$ values for centers W1 and W2 are closer to that found for $TiO_2$ than for the other hosts. Furthermore, all $nd^1$ ions previously studied in KTP have been found at the Ti sites and all have $g_x, g_y > g_z$ and $|A_x|, |A_y| < |A_z|$ (Table II), where $|A_z|$ is measured nearly along the shortest Ti-O bond for vanadium[21] and molybdenum,[24] as obtained here for centers W1 and W2. These results confirm that the centers observed here are due to $W^{5+}$ ions substituting for titanium.

In addition to pentavalent tungsten, other valence states of this impurity can be inferred from the behavior of the EPR signals under thermal treatments of the KTP samples (see Fig. 3). First, the strong increase of center W1 upon reduction [Fig. 2(b)] indicates the presence of a considerable amount of diamagnetic $W^{6+}$ ions at the Ti1 site for the as-grown samples. Hexavalent impurities are likely incorporated to the crystals since $WO_3$ powder was added to the growth flux (see Sec. III). Thus one of the electrons left by the oxygen lost in the reduction treatment[18] can be trapped by $W^{6+}$ to produce a paramagnetic $W^{5+}$ ion. Subsequent oxidation of the samples gives rise to the inverse effect, as deduced from the uniform decrease of the intensity of group W1 in Fig. 3. Besides, all tungsten impurities at the Ti1 site seem to be hexavalent for long oxidation periods, since the $W^{5+}$ signal disappears. On the contrary, the behavior of group W2 ($W^{5+}$ at the Ti2 site) is more complex. The intensity evolution under oxidation treatment (Fig. 3) suggests that some $W^{4+}$ is created at the Ti2 sites when reducing the samples. The intensity increase of the W2 signal for short oxidation periods would then indicate the production of more paramagnetic $W^{5+}$ ions at the expense of tetravalent tungsten. Moreover, long treatment periods would further oxidize $W^{5+}$ ions to the hexavalent state, giving rise to the observed intensity decrease of the W2 signal. It should be pointed out that $W^{4+}$ ($5d^2$) ions can be paramagnetic. However, no new resonances were observed which could be attributed to them. Besides, to our

TABLE II. Summary of experimental EPR data for $W^{5+}$ complexes in a variety of hosts, and for several $nd^1$ ions in KTP.

| Host (or solvent) | Complex | Center | $g_x$ | $g_y$ | $g_z$ | $\bar{g}$[a] | $\lvert A_x\rvert$[c] | $\lvert A_y\rvert$[c] | $\lvert A_z\rvert$[c] | $\lvert A_{iso}\rvert$[b] | Ground state | Ref. |
|---|---|---|---|---|---|---|---|---|---|---|---|---|
| $TiO_2$ | $[WO_6]^{7-}$ | $W^{5+}$ | 1.473 | 1.443 | 1.594 | 1.503 | 40.8 | 63.7 | 92.5 | 65.7 | $\lvert d_{xy}\rangle$ | 30 |
| $SnO_2$ | $[WO_6]^{7-}$ | $W^{5+}$ | 1.671 | 1.500 | 1.732 | 1.634 | 48.3 | 55.9 | 96.9 | 67.0 | $\lvert d_{xy}\rangle$ | 33 |
| $GeO_2$ | $[WO_6]^{7-}$ | $W^{5+}$ | 1.708 | 1.554 | 1.791 | 1.684 | 39.9 | 53.2 | 93.6 | 62.2 | $\lvert d_{xy}\rangle$ | 34 |
| (Glycerine) | $[W(CN)_8]^{3-}$ | $W^{5+}$ | 1.968 | 1.982 | 1.972 | | 68.5 | | 18.7 | 51.9 | $\lvert d_{3z^2-r^2}\rangle$ | 35 |
| $CaWO_4$ | $[WO_4]^{3-}$ | $W^{5+}$ | 1.587 | 1.60 | 1.850 | 1.679 | 53 | 66 | 19.1 | 46 | $\lvert d_{3z^2-r^2}\rangle$ | 36 |
| $WO_3$ | $[WO_6]^{7-}$ | $W^{5+}(\Psi)$ | 1.554 | 1.685 | 1.566 | 1.602 | 20 | 16 | 36 | 24 | $\lvert d_{xy}\rangle$ | 37 |
| $Cs_2ZrCl_6$ | $[WCl_6]^-$ | $W^{5+}$ | 1.767 | 1.811 | 1.782 | | 63.1 | | 124.7 | 83.6 | [d] | 38 |
| $Cs_2HfCl_6$ | $[WCl_6]^-$ | $W^{5+}$ | 1.765 | 1.810 | 1.780 | | 65 | | 124 | 84.7 | [d] | 38 |
| (MeCN/DMF) | $[WO(SPh)_4]^-$ | $WO^{3+}$ | 1.903 | 2.018 | 1.941 | | 44.4 | | 78.1 | 55.6 | $\lvert d_{xy}\rangle$ | 39 |
| (MeCN/DMF) | $[WO(SePh)_4]^-$ | $WO^{3+}$ | 1.923 | 2.086 | 1.977 | | 43.3 | | 74.0 | 53.5 | $\lvert d_{xy}\rangle$ | 39 |
| $K_2[WO(NCS)_5]$ | $[WO(NCS)_5]^{2-}$ | $WO^{3+}$ | 1.819 | 1.775 | 1.804 | | 75 | | 129 | 93 | [d] | 40 |
| Phosphate glass | | $WO^{3+}$ | 1.745 | 1.605 | 1.698 | | 72 | | 166 | 103 | [d] | 40 |
| $K_2SnF_6 \cdot H_2O$ | $[WOF_5]^{2-}$ | $WO^{3+}$ | 1.685 | 1.555 | 1.642 | | 94 | | 161 | 116 | $\lvert d_{xy}\rangle$ | 41 |
| $(NH_4)_2GeF_6$ | $[WOF_5]^{2-}$ | $WO^{3+}$ | 1.672 | 1.559 | 1.634 | | 87.4 | | 156.4 | 110.4 | $\lvert d_{xy}\rangle$ | 42 |
| KTP | $[WO_6]^{7-}$ | $WO^{3+}$ (W1) | 1.604 | 1.541 | 1.463 | 1.536 | 77 | 92 | 136 | 102 | $\lvert d_{xy}\rangle$ | This work |
| KTP | $[WO_6]^{7-}$ | $WO^{3+}$ (W2) | 1.606 | 1.564 | 1.505 | 1.558 | 82 | 97 | 151 | 110 | $\lvert d_{xy}\rangle$ | This work |
| KTP | $[MoO_6]^{7-}$ | $Mo^{5+}$[e] | 1.905 | 1.857 | 1.837 | 1.866 | 64 | 76 | 86 | 75 | [d] | 24 |
| KTP | $[VO_6]^{8-}$ | $VO^{2+}$ (1) | 1.981 | 1.975 | 1.937 | 1.964 | 50.6 | 60.8 | 175.4 | 96.5 | $\lvert d_{xy}\rangle$ | 21 |
| KTP | $[VO_6]^{8-}$ | $V^{4+}$ (I)[f] | | | 1.939 | | | | 168 | | [d] | 22 |
| KTP | $[VO_6]^{8-}$ | $V^{4+}$ (II)[f] | 1.959 | 1.938 | 1.952 | | 53.3 | | 166 | 90.9 | [d] | 22 |
| KTP | $[VO_6]^{8-}$ | $V^{4+}$ (I)[f] | 1.983 | 1.966 | 1.934 | 1.961 | 53.2 | 60.3 | 166.6 | 93.4 | [d] | 23 |
| KTP | $[VO_6]^{8-}$ | $V^{4+}$ (II)[f] | 1.973 | 1.960 | 1.937 | 1.957 | 53.7 | 61.0 | 168.3 | 94.3 | [d] | 23 |
| KTP | $[TiO_6]^{9-}$ | $Ti^{3+}(\Psi)$ | 1.946 | 1.872 | 1.771 | 1.863 | 8.0 | 11.0 | 26.7 | 15.2 | $\lvert d_{3z^2-r^2}\rangle$[g] | 13 |

[a] $\bar{g} = (g_x + g_y + g_z)/3$.

[b] $A_{iso} = (A_x + A_y + A_z)/3$.

[c] HF parameters in units of $10^{-4}$ cm$^{-1}$. Theory shows that the $A$ values of W centers must be negative (see text).

[d] Ground state not assigned in original work, but is probably $|d_{xy}\rangle$, as discussed in the text.

[e] Assigned to the molybdenyl $MoO^{3+}$ ion in the text.

[f] Should be very likely assigned also to the $VO^{2+}$ ion.

[g] Should be probably assigned to $|d_{xy}\rangle$, as discussed in the text.

knowledge detection of this ion by means of EPR has not been reported.

The presence of more highly charged cations (6+ and 5+) in the $Ti^{4+}$ sites of KTP must lead to a balancing charge compensation. The possible ways that charge compensation can take place are (a) via trivalent impurity cations located at the Ti sites and/or tetravalent impurities at the P sites, or (b) via cation vacancies. Mechanism (a) must be acting since for our as-grown samples $Rh^{3+}$ at the Ti sites[19] and $Si^{4+}$ at the P sites[10] have been found by spectrochemical analysis at the same concentration level as the hexavalent tungsten impurities (see Sec. III). On the other hand, mechanism (b) should also be active because of the large concentration of K vacancies found in our KTP samples (Sec. III). In fact, for KTP crystals containing 8% of $Nb^{5+}$ ions at the Ti sites, the charge compensation has been ascribed to the observed K deficiency.[43] Thus charge compensation mechanisms (a) and (b) seem to be equally active in our samples. The possibility of compensating impurity cations close to tungsten impurities cannot be elucidated here through the orientation of the axes of the **g** and **A** matrices because of the intrinsic low symmetry of the Ti sites. Light could be thrown on this question by studying W-doped KTP crystals with low concentration levels of other impurities and by comparing the results to those obtained here.

### C. Nature of the paramagnetic centers

A full analysis of the observed $g$ and $A$ values for the ground state of the $W^{5+}$ ions in KTP would be very difficult because of the lack of experimental information about the crystal field parameters and the spin-orbit coupling constant, as well as due to the difficulty of including covalence, which should be important for a $5d$ ion. Moreover, the local crystal field acting on the $W^{5+}$ ions is of such a low symmetry that a complete interpretation of the spin-Hamiltonian parameters would be a very complex issue. However, simple considerations will be used in what follows to obtain general trends about the nature of the paramagnetic centers.

#### 1. *Ground-state assignment*

The free ion $W^{5+}$ has a fivefold orbital degeneracy which is first split by an octahedral cubic field into a ground triplet level and an excited doublet level. With the additional tetragonal distortion and lower symmetry components of the crystal field at the Ti sites, the ground orbital triplet splits into three orbital singlets described by wave functions with main character $|d_{xz}\rangle$, $|d_{yz}\rangle$, and $|d_{xy}\rangle$, respectively. It should be noted that $x$, $y$, and $z$ are considered here forming a reference frame which points towards the ligands for a high-symmetry case and, as mentioned above, are not simply related to the principal axes of Table I. In most cases the $W^{5+}$ ion has been found in octahedral sites with tetragonal compression along a $z$ axis, so that the orbital ground state mainly has $|d_{xy}\rangle$ character (see Table II). For the unpaired electron located in such an orbital and considering $C_{4v}$ symmetry with $z$ as the fourfold axis, the HF interaction can be accounted for to a first approximation by[32,34,44]

$$A_z \approx P(-\kappa - 4/7)\ ; \quad A_x = A_y \approx P(-\kappa + 2/7)\ , \qquad (2)$$

where the isotropic contact HF contribution is given by $-P\kappa$ (equal to $-K$ in Ref. 32) and the anisotropic part is the first-order approximation of the electron-nuclear dipolar contribution, being $P = 2g_n\beta\beta_n\langle r^{-3}\rangle$ (Ref. 27) and $\kappa$ the core polarization parameter. Since for transition metal ions $\kappa$ is normally a positive parameter,[27,35] $|A_x|$ and $|A_y|$ will be always smaller than $|A_z|$ for all cases with a $|d_{xy}\rangle$-based ground state, as observed in Table II. It must be pointed out that the HF constants will be negative, as $g_n$ is positive for $^{183}W$. The observation of $|A_z| > |A_x|, |A_y|$ for the $W^{5+}$ ions in KTP and the fact that the principal $z$ axis of the **A** matrices has been found in Sec. V A to be roughly parallel to the direction of the compression along the shortest Ti-O bonds, both agree with a $|d_{xy}\rangle$-based ground state.

On the other hand, the ordering of the principal $g$ values with regard to the ordering of the principal $A$ values also supports the previous ground-state assignment, as explained next. Although for the $W^{5+}$ ions in KTP the principal axes of the **g** and **A** matrices are noncoincident, we can associate the principal values according to the closest axes, as done in Table I. Assuming this association, we obtain that the smallest $g$ value corresponds to the largest $A$ value. This correlation has also been found, experimentally, for the centers of vanadium and molybdenum in KTP (Table II and Refs. 21 and 24). The same relationship takes place along the compression axis of the oxygen octahedra which surrounds $V^{4+}$ ($3d^1$) ions at the interstitial sites of $TiO_2$ (Refs. 45, 46, and 33). In that case, a $|d_{xy}\rangle$-based ground state has been established. Hence the observed correlation for centers W1 and W2, as well as for vanadium and molybdenum in KTP, strongly supports the assignment of a $|d_{xy}\rangle$-based ground state for all these $nd^1$ ions. It is interesting to mention here the case of the center $\Psi$ of $Ti^{3+}$ in KTP (Table II and Ref. 13). Although the principal axis for the largest $A$ value has not been obtained close to a short Ti-O bond direction,[13] a similar correlation holds for the spin-Hamiltonian parameters of this center (Table II). This points also to a $|d_{xy}\rangle$ ground state for the $Ti^{3+}$ centers in KTP, in contrast to a $|d_{3z^2-r^2}\rangle$ state proposed in Ref. 13.

#### 2. *The tungstenyl ion in* KTP

Since $V^{4+}$ has been found in KTP forming the vanadyl $VO^{2+}$ ion,[21] we must consider the possibility that pentavalent tungsten be present in KTP as the tungstenyl $WO^{3+}$ ion. This should be favored by the existence of the short "titanyl" bond for both Ti sites. It is well known[47] that the high oxidation states of metal ions at the beginning of the transition series have a remarkable capacity to form oxycations with the general formula $MO^{n+}$. Among these, the vanadyl ion is one of the simplest and most stable ions of this type. Also it has been the most widely investigated.[32,44,47–49] The oxycations in

different complexes show typical electronic and magnetic properties due to the short and strong M-O bond. In fact, the unpaired electron in the $nd^1$ oxycations is always located in the $|d_{xy}\rangle$ orbital, which is nonbonding or slightly $\pi$ antibonding with the equatorial ligands.[44,47,48]

As discussed above, the $|d_{xy}\rangle$ orbital is also the ground state for the W centers in KTP, which agrees with the existence of the tungstenyl ion in our case. In order to confirm this, we first note the results of McGarvey,[32] who found values of the core polarization parameter $\kappa$ for the oxycations $VO^{2+}$, $NbO^{2+}$, and $MoO^{3+}$ about 1.6 times larger than for $V^{4+}$, $Nb^{4+}$, and $Mo^{5+}$, respectively. The increase in the values of $\kappa$ could be ascribed to polarization effects involving the bonding electrons in the M-O bond,[32] but also to indirect contribution to $\kappa$ from the $|(n+1)s\rangle$ empty orbital.[48] The different values of $\kappa$ for the metal ion and the corresponding oxycation would allow to distinguish between them. However, the difficult determination of reliable values of $\kappa$ for pentavalent tungsten,[34] makes this method inapplicable in our case.

The criterion employed here makes use of the linear relation which arises by plotting the experimental mean $g$ value $\bar{g}$ versus the isotropic HF constant $A_{iso}$ for various hosts (see Table II for definitions of $\bar{g}$ and $A_{iso}$). The data appear arranged along two different straight lines for the metal and the oxycation. This has been reported for the case of $V^{4+}$ and $VO^{2+}$ ions.[49] The experimental EPR data for tungsten are more scarce than for vanadium,[49] but enough examples are collected in Table II of both $W^{5+}$ and $WO^{3+}$ ions to obtain reliable linear dependences. These are shown in Fig. 6, where $|A_{iso}|$ is expressed in gauss. The linear dependences are explained by means of[32,48,49]

$$A_{iso} = -P\kappa + P(\bar{g} - 2.0023) , \tag{3}$$

assuming that the parameter $\kappa$ depends linearly on $\bar{g}$ through $P\kappa = P\kappa_0 - \alpha_i(\bar{g} - 2.0023)$, being $i = 1$ for $W^{5+}$ and 2 for $WO^{3+}$ (Ref. 49). Thus the slope of the straight lines fitted in Fig. 6 is $-1/P_i$, where $P_i = P + \alpha_i$. It must be mentioned that some of the data in Table II have been excluded in Fig. 6 for various reasons. On the one hand, the $A_{iso}$ values for $W^{5+}$ in $WO_3$ and $CaWO_4$ are found too little because the equality of the W lattice ions facilitates large delocalization of the unpaired electron.[37] On the other hand, although the data for the chlorides in Table II closely fall on the straight line for the $WO^{3+}$ ions in Fig. 6, the centers have not been ascribed to the tungstenyl ion in the original work.[38] Thus, since the EPR data for centers W1 and W2 are close to the $WO^{3+}$ line, pentavalent tungsten in KTP is identified as the tungstenyl $WO^{3+}$ ion.

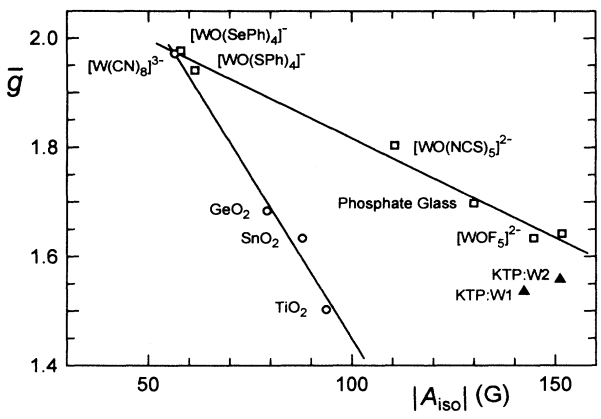


FIG. 6. Relation of mean $g$ values $\bar{g}$ versus isotropic HF constants $|A_{iso}|$ for $W^{5+}$ ions (○) and for $WO^{3+}$ ions (□) in several hosts (see Table II). Each data set is fitted to the linear relation $\bar{g} = -|A_{iso}|/P_i + (P\kappa_0/P_i + 2.0023)$ (see text). The fits provide $P_1 = 83.4$ G, $(P\kappa_0)_1 = 53.9$ G for $W^{5+}$ and $P_2 = 275.6$ G, $(P\kappa_0)_2 = 48.9$ G for $WO^{3+}$. The data for centers W1 and W2 in KTP are represented with full triangles.

The $A_{iso}$ values for centers W1 and W2 are, however, somewhat smaller than expected from the tendency of the $WO^{3+}$ line. This can be explained taking into account that the data used to obtain that line correspond to complexes in tetragonal symmetry (Table II), where mixing of the $|5d_{xy}\rangle$ orbital and the empty $|6s\rangle$ orbital is not allowed.[32] However, in a low-symmetry case, as tungsten in KTP, such mixing is allowed, giving a direct $|6s\rangle$ contribution to $\kappa$ of opposite sign to the indirect $|6s\rangle$ contribution mentioned above.[48] Moreover, as the distortion from cubic symmetry of the $(Ti1)O_6$ octahedron is larger than that for $(Ti2)O_6$ (Ref. 25), this could explain a larger $|6s\rangle$ mixing for center W1 (Ti1 site) than for W2 (Ti2 site), thus giving rise to a smaller $A_{iso}$ value for center W1, as observed.

Finally, $Mo^{5+}$ ions in KTP (Ref. 24) are also expected to be present in the form of the molybdenyl $MoO^{3+}$ ion because of the similarities with the vanadyl and tungstenyl ions (Table II). This identification is supported by the fact that the $A_{iso}$ value of pentavalent Mo is larger in KTP than in many other hosts,[32,34,39] as found here for the tungstenyl ion in KTP.

### 3. *Comparison with other oxycations in* KTP

In addition to the analogies found in the EPR parameters of all $nd^1$ ions in KTP (Table II) other trends appear on the SHF structure of the spectra as well as on the different occupation degree of the Ti1 and Ti2 sites by the impurities, which may give further information about the nature of the oxycations in KTP.

The SHF structure in the EPR spectra of the vanadyl ion in KTP has been attributed to interaction with $^{31}P$ nuclei.[21] This structure resembles very much that exhibited by the tungsten signals described in Sec. IV A. For both oxycations the signals corresponding to the Ti1 site show a doublet structure with a separation of about 4 G for $VO^{2+}$ (Ref. 21) and around 14 G for $WO^{3+}$ (Sec. IV A). Whereas, the signals for the Ti2 site have a triplet structure, the separation being about 7 G for $VO^{2+}$ (Ref. 21) and around 17 G for $WO^{3+}$ (Sec. IV A).

In the case of the molybdenyl ion, the SHF structure observed on the Mo signals has been attributed to interaction with the $^{39}K$ and $^{41}K$ isotopes.[24] However, we believe it should be also ascribed to interaction with $^{31}P$ nuclei, since the nuclear magnetic moment is about 10 times larger for $^{31}P$ than for the odd K isotopes. Besides,

the K sites are located farther away from the Ti sites (3.6 Å is the shortest Ti-K distance) than the P sites (around 3.2 Å).[25] Thus from the Mo spectra shown in Fig. 1 of Ref. 24 we estimate a typical phosphorous SHF splitting of about 10 G. This value falls between the observed splittings of 4–7 G for $VO^{2+}$ and 14–17 G for $WO^{3+}$. The existence of SHF structure indicates some $\pi$-antibonding character of the $|d_{xy}\rangle$-based ground state of the three oxycations.[44,48] Furthermore, assuming that the unpaired spin density is transferred to phosphorous in the same way for the three cases, it is clear that the covalence increases in the order V < Mo < W. An analogous ordering has been found for the fluorocomplexes $[CrOF_5]^{2-}$, $[MoOF_5]^{2-}$, and $[WOF_5]^{2-}$ (Ref. 41). The observed ordering supports the identification of the common oxycation nature of vanadium, molybdenum, and tungsten centers located at the Ti sites of KTP.

Finally, we will comment on the higher concentration of tungsten impurities at the Ti1 site of KTP than at the Ti2 site, as can be inferred from the behavior of the signals under thermal treatments (Sec. IV B). This result is similar to those found for other oxycations in KTP. Doping the crystals with $V_2O_4$, the occupation ratio Ti1:Ti2 by $VO^{2+}$ ions is found by EPR close to 10:1 (Ref. 21). Also, for an 8% concentration of diamagnetic $Nb^{5+}$ ions in KTP, which are found at the Ti sites, a ratio close to 5:1 is determined by means of x-ray powder-diffraction analysis.[43] The $Nb^{5+}$ ions are also expected to be forming an oxycation ($NbO^{3+}$ ion) since the analysis of Thomas and Watts[43] shows that the shortest Nb-O bonds are still "anomalously short" ($\approx$1.76 Å). Moreover, although thermal treatments have not been carried out on Mo-doped KTP crystals,[24] a three-times higher concentration of pentavalent Mo was found for center II than for center I. Contrary to the assignment made in Ref. 24, we would locate center I at the Ti2 site, since the $z$ axis of this center (with polar coordinates $\theta=33°$, $\phi=64°$) (Ref. 24) is very close to the principal $z$ axis of the **A** matrix for the tungsten center W2 here measured ($\theta=35°$, $\phi=68°$ in Table I). Consequently, we would locate center II at the Ti1 site. Thus it seems feasible to conclude that the molybdenyl ion also presents lower occupation of the Ti2 site. On the contrary, we have found by means of thermal treatments that the impurity ions $Fe^{3+}$ (Refs. 19,20) and $Rh^{2+}$ (Ref. 19), which are also present in our samples, show similar occupation levels in both Ti sites.[19] Therefore, the higher occupation of the Ti1 site seems to be concerned with the oxycation nature of the center.

The higher preference for the Ti1 site shown by the vanadyl ion has been attributed[21] to the fact that the "titanyl" Ti1-OT2 bond is significantly shorter (1.716 Å) than the "titanyl" Ti2-OT1 bond (1.733 Å).[25] This could also explain the higher occupation of the Ti1 site shown by the $Nb^{5+}$ ions, as the shortest Nb-O distances are 1.752 and 1.775 Å for the Ti1 and Ti2 sites, respectively.[43] However, in this latter work it is proposed[43] that the lower occupation of the Ti2 site is due to the existence of shorter K-Ti distances for this site, which should produce a higher repulsion at the Ti2 site than at the Ti1 site. This reasoning could also explain that hexavalent tungsten seems to be incorporated at the Ti1 site in a much higher proportion than pentavalent niobium, owing to the additional positive charge. Both structural peculiarities of the Ti sites could make the Ti1 site energetically more favorable for the oxycation formation.

However, we believe that the different abilities to relax of the oxygen environments of the Ti sites when the impurity replaces titanium can be of greater importance than the former reasonings. In particular, the role of the four equatorial ligands on the length and strength of the short bond in the oxycations has been shown to be very important.[48] By comparing the crystallographic data for KTP (Ref. 25) to those for Nb-doped KTP (Ref. 43) and the isostructural $KVOPO_4$ (Ref. 50), one finds that substitution of titanium by niobium or vanadium produces only a slight relaxation of the four equatorial oxygens around Ti2, which belong to $PO_4$ groups (see Fig. 1). However, two of the four equatorial oxygens around Ti1 undergo a considerable relaxation in both cases. These are OT1 and O6 in Fig. 1, noting that OT1 does not belong to any $PO_4$ group and that O6 is the only oxygen which is not coordinated to any potassium.[50] From these structural results it appears that the $(Ti1)O_6$ octahedron shows less rigidity than the $(Ti2)O_6$ octahedron upon oxycation formation. This probably implies a smaller energy and, consequently, a larger preference of the oxycations for the Ti1 site.

## ACKNOWLEDGMENTS

This work has been partially supported by CICyT (Spain) under Grants No. MAT93-0707 and No. MAT93-1267E. The assistance of A. Cintas in sample preparation and of M. J. Martín in performing thermal treatments are gratefully acknowledged.

[1]J. D. Bierlein and H. Vanherzeele, J. Opt. Soc. Am. B **6**, 622 (1989).

[2]F. C. Zumsteg, J. D. Bierlein, and T. E. Gier, J. Appl. Phys. **47**, 4980 (1976).

[3]M. G. Roelofs, A. Ferretti, and J. D. Bierlein, J. Appl. Phys. **73**, 3608 (1993).

[4]L. Zhang, P. J. Chandler, P. D. Townsend, Z. T. Alwahabi, S. L. Pityana, and A. J. McCaffery, J. Appl. Phys. **73**, 2695 (1993).

[5]A. A. Ballman, H. Brown, D. H. Olson, and C. E. Rice, J. Cryst. Growth **75**, 390 (1986).

[6]D. P. Shumov, V. S. Nikolov, K. N. Iliev, and A. L. Aleksandrovskii, Cryst. Res. Technol. **25**, 1245 (1990).

[7]C. G. Chao, Q. Z. Qiang, T. G. Kui, S.W. Bao, and T. H. Gao, J. Cryst. Growth **112**, 294 (1991).

[8]D. P. Shumov, M. P. Tarassov, and V. S. Nikolov, J. Cryst. Growth **129**, 635 (1993).

[9]T. F. McGee, G. M. Blom, and G. Kostecky, J. Cryst. Growth **109**, 361 (1991).

[10]P. A. Morris, A. Ferretti, J. D. Bierlein, and G. M. Loiacono,

J. Cryst. Growth **109**, 367 (1991).
[11]R. Blachman, P. F. Bordui, and M. M. Fejer, Appl. Phys. Lett. **64**, 1318 (1994).
[12]G. M. Loiacono, D. N. Loiacono, T. McGee, and M. Babb, J. Appl. Phys. **72**, 2705 (1992).
[13]M. G. Roelofs, J. Appl. Phys. **65**, 4976 (1989).
[14]L. K. Cheng, J. D. Bierlein, and A. A. Ballman, J. Cryst. Growth **110**, 697 (1991).
[15]I. Tordjman, R. Masse, and J. C. Guitel, Z. Kristallogr. **139**, 103 (1974).
[16]G. J. Edwards, M. P. Scripsick, L. E. Halliburton, and R. F. Belt, Phys. Rev. B **48**, 6884 (1993).
[17]M. P. Scripsick, G. J. Edwards, L. E. Halliburton, R. F. Belt, and G. M. Loiacono, J. Appl. Phys. **76**, 773 (1994), and references therein.
[18]M. J. Martín, D. Bravo, R. Solé, F. Díaz, F. J. López, and C. Zaldo, J. Appl. Phys. **76**, 7510 (1994).
[19]D. Bravo, M. J. Martín, J. Gavaldá, F. Díaz, C. Zaldo, and F. J. López, Phys. Rev. B **50**, 16224 (1994), and references therein.
[20]J. M. Gaite, J. F. Stenger, Y. Dusausoy, G. Marnier, and H. Rager, J. Phys. Condens. Matter **3**, 7877 (1991).
[21]A. B. Vassilikou-Dova, S. Jansen, F. Wallrafen, and G. Lehmann, Z. Naturforsch. **44a**, 711 (1989).
[22]I. N. Geifman, P. G. Nagornyi, A. N. Usov, and Pham za Ngy, Sov. Phys. Solid State **33**, 1535 (1991).
[23]S. Han, J. Wang, Y. Xu, Y. Liu, and J. Wei, J. Phys. Condens. Matter **4**, 6009 (1992).
[24]I. N. Geifman, A. N. Usov, and P. G. Nagornyi, Phys. Status Solidi B **172**, K73 (1992).
[25]P. A. Thomas, A. M. Glazer, and B. E. Watts, Acta Crystallogr. Sect. B **46**, 333 (1990).
[26]J. R. Pilbrow and M. R. Lowrey, Rep. Prog. Phys. **43**, 433 (1980).
[27]A. Abragam and B. Bleaney, *Electron Paramagnetic Resonance of Transition Ions* (Clarendon, Oxford, 1970).
[28]M. A. Hitchman, C. D. Olson, and R. L. Belford, J. Chem. Phys. **50**, 1195 (1969).
[29]J. R. Pilbrow and M. E. Winfield, Mol. Phys. **25**, 1073 (1973).
[30]T. T. Chang, Phys. Rev. **147**, 264 (1966).
[31]J. R. Pilbrow, *Transition Ion Electron Paramagnetic Resonance* (Clarendon, Oxford, 1990), Appendix P.
[32]B. R. McGarvey, J. Phys. Chem. **71**, 51 (1967).
[33]P. Meriaudeau, Y. Boudeville, and P. de Montgolfier, Phys. Rev. B **16**, 30 (1977).
[34]D. P. Madacsi, M. Stapelbroek, R. B. Bossoli, and O. R. Gilliam, J. Chem. Phys. **77**, 3803 (1982), and references therein.
[35]B. R. McGarvey, Inorg. Chem. **5**, 476 (1966).
[36]Y. G. H. Azarbayejani, Bull. Am. Phys. Soc. **10**, 1131 (1965).
[37]O. F. Schirmer and E. Salje, Solid State Commun. **33**, 333 (1980).
[38]S. Maniv, W. Low, and A. Gabay, J. Phys. Chem. Solids **32**, 815 (1971).
[39]G. R. Hanson, G. L. Wilson, T. D. Bailey, J. R. Pilbrow, and A. G. Wedd, J. Am. Chem. Soc. **109**, 2609 (1987).
[40]R. S. Abdrakhmanov and T. A. Ivanova, Fiz. i Khim. Stekla **2**, 15 (1976) [Sov. J. Glass Phys. Chem. **2**, 12 (1976)].
[41]J. T. C. van Kemenade, Rec. Trav. Chim. **89**, 1100 (1970).
[42]J. T. C. van Kemenade, Rec. Trav. Chim. **92**, 1102 (1973).
[43]P. A. Thomas and B. E. Watts, Solid State Commun. **73**, 97 (1990).
[44]K. DeArmond, B. B. Garrett, and H. S. Gutowsky, J. Chem. Phys. **42**, 1019 (1965).
[45]F. Kubec and Z. Sroubek, J. Chem. Phys. **57**, 1660 (1972).
[46]P. de Montgolfier, P. Meriaudeau, Y. Boudeville, and M. Che, Phys. Rev. B **14**, 1788 (1976).
[47]C. J. Ballhausen and H. B. Gray, Inorg. Chem. **1**, 111 (1962).
[48]L. J. Boucher, E. C. Tynan, and T. F. Yen, in *Electron Spin Resonance of Metal Complexes,* edited by Teh Fu Yen (Plenum, New York, 1969), p. 111.
[49]T. Hirose, M. Kawaminami, and M. Arakawa, J. Phys. Soc. Jpn. **54**, 3584 (1985).
[50]M. L. F. Phillips, W. T. A. Harrison, T. E. Gier, G. D. Stucky, G. V. Kulkarni, and J. K. Burdett, Inorg. Chem. **29**, 2158 (1990).